View Online / Journal Homepage / Table of Contents for this issue
Dynamic Article Links

Journal of Materials Chemistry

Cite this: J. Mater. Chem., 2012, 22, 18051

www.rsc.org/materials

PAPER

# Enhanced charge-carrier mobility in polymer nanofibers realized by solvent-resistant soft nanolithography†

**Elisa Mele,*[a] Francesca Lezzi,[ab] Alessandro Polini,‡[c] Davide Altamura,[d] Cinzia Giannini[d] and Dario Pisignano*[abc]**

***Received 5th June 2012, Accepted 9th July 2012***
**DOI: 10.1039/c2jm33611a**



We realize nanofibers of regioregular poly(3-hexylthiophene) (P3HT) by solvent-resistant nanolithography and use them as the active medium in organic field effect transistors. This process favors a remarkable improvement of the device performances, since we exploit the nanofluidic flow in perfluoropolyether capillaries and the slow solvent evaporation rate in the mold cavities to induce the reorganization of the P3HT chains and obtain a charge carrier mobility 60 times higher than in the corresponding homogenous films. The precise control of the structure cross-section (sub-100 nm) and of the spatial arrangement on the transistor electrodes is very promising for the development of one-dimensional (1D) nanostructures of conjugated materials with high field-effect mobility, applicable to miniaturized optoelectronic devices.

Organic field-effect transistors (OFETs) based on solution-processed conjugated polymers are considered key devices for flexible electronics, due to their characteristics of simple fabrication, large-area processing, and low-cost.[1] However, OFETs performances often suffer because of the relatively low charge mobility of organic semiconductors, which in turn is affected by the degree of regioregularity, by the structural chain order, the molecular weight, and the deposition conditions.[2] Aiming to increase the charge carrier mobility in organic compounds and improve the transistor performances, various nanofabrication approaches are employed, mainly by inducing a more ordered molecular packing through nanorubbing,[3] electrospinning,[4] nanoimprint[5,6] or soft lithography.[7,8] Zheng *et al.* have demonstrated the alignment of the liquid-crystalline polymer, poly(9,9-dioctylfluorene-co-benzothiadiazole), into nanochannels by nanoimprint lithography (NIL), enhancing the mobility by about a factor of 2.[9] NIL has been also applied by Cui *et al.*[5] to pattern regioregular poly(3-hexylthiophene) (P3HT), improving the hole mobility by using gratings with a period of 700 nm. Hu *et al.* have developed an embossing procedure using hard molds at room temperature for producing nanowires of conjugated polymers, such as poly(3,3‴-didodecyl-quaterthiophene).[6] Furthermore, P3HT transistor channels have been fabricated by lithographically controlled wetting,[7] or defined onto gate dielectrics patterned by microcontact printing.[8]

Unfortunately, with very few exceptions,[5,7] the increase of mobility achieved so far is quite low, often well below one order of magnitude. The nanoscale layer of conjugated polymer, remaining underneath the channel features upon patterning, is especially detrimental to the device performance,[7] and this bottom layer is hardly removed by either NIL methods or soft lithographies using conventional silicone-based elastomers such as polydimethylsiloxane (PDMS). Indeed, PDMS is largely incompatible with solution-processing of conjugated polymers, as it undergoes dramatic swelling in non-polar solvents.[10]

In this work, we demonstrate a significant improvement of the performances of OFETs based on arrays of spatially separated, sub-100 nm P3HT features. These are produced by the solvent-resistant soft lithographic approach, known as particle replication in non-wetting templates,[11] which exploits the nanofluidic flow in non-swelling capillaries made by perfluoropolyether (PFPE). The obtained P3HT features exhibit a field-effect mobility 60 times higher than that of homogeneous films, as an effect of the patterning process. The low surface energy of the template is combined with the slow solidification of the conjugated polymer occurring while the solution is confined in the mold cavities. This process is permitted by the non-swelling behavior of the used PFPE–urethane methacrylate elastomers, and it results in a remarkable improvement of the charge carrier

[a]*Center for Biomolecular Nanotechnologies @UNILE, Fondazione Istituto Italiano di Tecnologia, via Barsanti, I-73010 Arnesano (LE), Italy. E-mail: elisa.mele@iit.it*
[b]*Dipartimento di Matematica e Fisica "Ennio De Giorgi", Università del Salento, via Arnesano, I-73100 Lecce, Italy. E-mail: dario.pisignano@unisalento.it*
[c]*National Nanotechnology Laboratory of Consiglio Nazionale delle Ricerche-Istituto Nanoscienze, Università del Salento, via Arnesano, I-73100 Lecce, Italy*
[d]*Istituto di Cristallografia (IC-CNR), via Amendola 122/O, 70126 Bari, Italy*

† Electronic supplementary information (ESI) available: Details about used materials, device fabrication, and performed characterizations. See DOI: 10.1039/c2jm33611a

‡ Present address: Materials Science Division, Lawrence Berkeley National Laboratory, 1 Cyclotron Road, Berkeley, CA 94720, USA.

transport. P3HT features with sizes of 80 nm and 270 nm are produced, and their morphological investigation evidences a precise control of the cross-section and of the spatial arrangement on the transistor electrodes. These results are especially promising for the development of one-dimensional (1D) nanostructures by conjugated materials,[12,13] that can exhibit high field-effect mobility and are applicable to miniaturized optoelectronic devices.

Highly regioregular P3HT, deposited by drop-casting or spin-coating, is known to self-organize into a well-ordered lamellar structure, with thiophene rings edge-on oriented relative to the substrate (*i.e.* facing each other with π–π stacking direction in the plane of the substrate).[14,15] Molecular reconfiguration mechanisms have been reported for P3HT molecules after NIL, performed at high temperature and pressure.[16,17] Other studies highlight that the molecular self-organization is affected by the rate of solvent evaporation in the liquid-to-solid transition during the film deposition.[18,19] A slow evaporation rate allows the P3HT chains to be better ordered, facilitating their self-assembling and determining the formation of defect-free structures.[18] In addition, the mobility of P3HT depends significantly on the used solvent, as a consequence of deposition discontinuities, polymer solubility and solvent properties.[20] The most commonly used solvent for device fabrication is chloroform, enabling hole mobilities up to 0.2 $cm^2\ V^{-1}\ s^{-1}$ to be achieved.[18] However, its fast evaporation is unfavorable for lithographic applications, which limits the realization of high-quality nanostructures. For this reason, we focus here on dichlorobenzene, obtaining field-effect mobilities for thin films of P3HT comparable to those reported in the literature ([1–4] × $10^{-3}\ cm^2\ V^{-1}\ s^{-1}$)[21,22] and then strongly improving performances by our lithographic technique.

We propose PFPE molds, previously used to fabricate arrays of isolated features and monodisperse organic micro- and nanoparticles with highly controlled shape and size,[11,23,25] as the best soft templates for fabricating conjugated polymer structures with high mobility. Because of the low surface energy (15 mN $m^{-1}$)[26] of PFPEs, target organic liquids deposited between a mold and a substrate do not wet the stamp surface, filling only recessed features and strongly favoring the production of nanostructures free of any interconnecting layer underneath. Moreover, using these molds with solutions of conjugated polymers allows us to take full advantage of the non-swelling properties of PFPE–urethane methacrylates in nonpolar solvents. Here, we also demonstrate the effectiveness of PFPE molds in improving the characteristics of P3HT transistors by the comparison with conventional elastomers, such as PDMS.

Our OFETs are fabricated by a bottom-contact architecture, with an n-type Si substrate as gate electrode, a 400 nm thick $SiO_2$ layer as dielectric, and Cr/Au layers as drain (D) and source (S) electrodes, produced by thermal evaporation through a shadow-mask. Before depositing the organic semiconductor, the devices are treated with dimethyldichlorosilane to obtain hydrophobic surfaces. Two different Si master structures for patterning, fabricated by electron-beam lithography, present 1 μm and 330 nm periodic grooves with a feature depth of 300 nm. The PFPE–urethane dimethacrylate molds are obtained by pouring the liquid precursor onto the masters, and subsequent photochemical crosslinking by UV light in nitrogen atmosphere. PDMS replicas are also produced by thermally curing the prepolymer onto the 1 μm period master, whereas 330 nm periodic features cannot be faithfully replicated in PDMS due to the well-known resolution limits of silicone elastomers.[27] A 1 μL droplet of a 0.2 mM dichlorobenzene solution of regioregular P3HT is deposited onto the electrode area, forming a liquid film on which the PFPE mold is placed with its features oriented perpendicularly to the D–S facing sides (Fig. 1a). With respect to other photocurable PFPE–urethane methacrylate elastomers,[24,26] the material used here is characterized by a higher molecular weight (about 4000 g $mol^{-1}$) and superior elastomeric character, thus favoring the stable, reversible sealing of the mold to the substrate during the patterning procedure. Indeed, we find that the relief regions in the stamp reversibly seal to the surface of $SiO_2$ and to the Au electrodes, shaping cavities in which the P3HT solution is tightly confined. After the complete evaporation of the solvent (at 50 °C over 2 hours under nitrogen), the mold is peeled off and an array of spatially separated P3HT features remains between the S and D electrodes of the transistor (Fig. 1b). Thermal annealing is then carried out at 150 °C for 5 min under $N_2$ atmosphere, for completely removing the solvent. The same lithographic procedure is carried out to print P3HT by PDMS replicas. However, differently from PFPE molds, PDMS elements swell and change shape when exposed to common organic solvents[10] including dichlorobenzene. The deformation of PDMS replicas placed onto the P3HT solution is clearly evident (Fig. S1†) and causes a loss of contact between the elastomeric features in relief and the substrate during printing, and consequently the presence of a residual organic layer between adjacent polymer nanostructures.[11] Further details on materials and fabrication procedures are available in the ESI.†

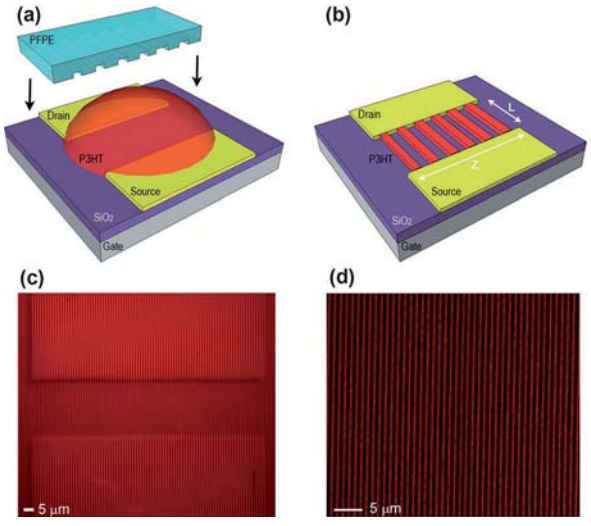


**Fig. 1** Process schematics (features not to scale). (a) Deposition of a droplet of dichlorobenzene P3HT solution and PFPE template positioning. (b) After mold peeling-off, an array of aligned and isolated P3HT features connect the S and the D electrodes. *L*: inter-electrodes gap distance, *Z*: corresponding width. (c) P3HT pattern with feature resolution of 270 nm on the entire device area (S and D Au electrodes are visible as broad rectangular regions underneath the bright polymer features) imaged by fluorescence microscopy, and (d) channel region of transistor patterned by 1 μm periodic structures, visualized by confocal microscopy.

 

Fig. 1c shows the surface of the OFET patterned by the 1 μm period PFPE mold, evidencing well aligned periodic features of P3HT. The pattern covers an area of about 0.5 $cm^2$, with feature length of a few mm, and extends both on the Au electrodes and across the gap, revealing the capability of the mold of fitting to the sample microscale morphology without lack of conformal contact. *No interconnecting bottom layer is visible between adjacent P3HT features* (Fig. 1d), *which is particularly useful to improve the device performance.* Polarized absorption, often used to probe molecular order as induced by nano-confinement,[9] is slightly more intense when the incident light is polarized parallel to the longitudinal axis of the features, and lower in the case of perpendicular polarization. By rotating the polarizer, we find that the absorption intensity changes following a squared-cosine dependence on the polarization angle, with maximum absorption for the light polarized parallel to the chain orientation.[28] The high quality of the pattern is also confirmed by scanning electron microscopy (SEM, Fig. 2), and by atomic force microscopy (AFM), providing information about the size and height of P3HT structures. The polymer features produced by the PFPE templates exhibit a height of about 300 nm, reproducing quite faithfully the starting masters. In particular, Fig. 2a and b show SEM planar views of P3HT structures, that have a size distribution well-fitted by a Gaussian curve peaked at 270 nm with a dispersion (full width at half maximum, FWHM) of about 10 nm (Fig. 2c). In Fig. 2d and e, we show the morphology of smaller polymeric features, having a size distribution peaked at 80 nm and a FWHM of about 16 nm (Fig. 2f). Hence, the solvent-resistant approach proves to be a simple and low-cost, soft lithographic method for the production of 1D sub-100 nm aligned structures with mm length and uniform width and height, starting from solution-processed organic semiconductors.

We compare the performances of the OFETs based on P3HT aligned features of 80 nm (Fig. 3a) and 270 nm (Fig. 3b), produced by PFPE molds, with those of analogous devices based on spin-cast films with a thickness of 300 nm (Fig. 3c) and on nanostructures replicated by PDMS elements (Fig. S2a†), as control. D–S current–voltage [$I_{ds}(V_{ds})$] characteristics for gate voltages ($V_{gs}$) from 0 to −100 V highlight the well-known p-type behavior of P3HT transistors, working in accumulation mode. We do not observe a complete current saturation at high $V_{ds}$ values, which is likely related to impurities induced in the polymer during the device fabrication.[4,21] These impurities determine an increased density of the residual holes in the transistor channel, and also affect the threshold voltage that tends to assume positive values. The corresponding transfer characteristics, $I_{ds}(V_{gs})$, and $|I_{ds}|^{1/2}(V_{gs})$ curves (for $V_{ds} = -100$ V), for structured and thin-film OFETs are displayed in Fig. 3d–f (and in Fig. S2b† for devices realized by PDMS). The characteristics indicate a threshold voltages ($V_{th}$) below 20 V. The saturation field-effect mobility, $\mu$, is estimated by the OFET characteristics according to the current behaviour, $I_{ds} = \frac{Z_{eff}}{2L} C\mu(V_{gs} - V_{th})^2$,[14] where $C$ is the gate dielectric capacitance per unit area (~8 nF $cm^{-2}$ for the thermally grown $SiO_2$),[24] $L$ is the transistor channel length (= 25 μm). The effective channel width, $Z_{eff}$, is given by the P3HT single-feature width times the number of D–S connecting features (for transistors patterned by PFPE molds), or by the full electrodes width, $Z = 100$ μm (for the thin films and for devices patterned by PDMS molds). The OFETs based on 80 nm features show mobility values of 0.1 $cm^2\ V^{-1}\ s^{-1}$, which is higher by a factor 60 compared to that of film devices ($1.7 \times 10^{-3}$ $cm^2\ V^{-1}\ s^{-1}$). Moreover, the electrical conductivity ($\sigma$) of 80 nm P3HT features is about $1.6 \times 10^{-1}$ S $m^{-1}$, that is 53 times higher

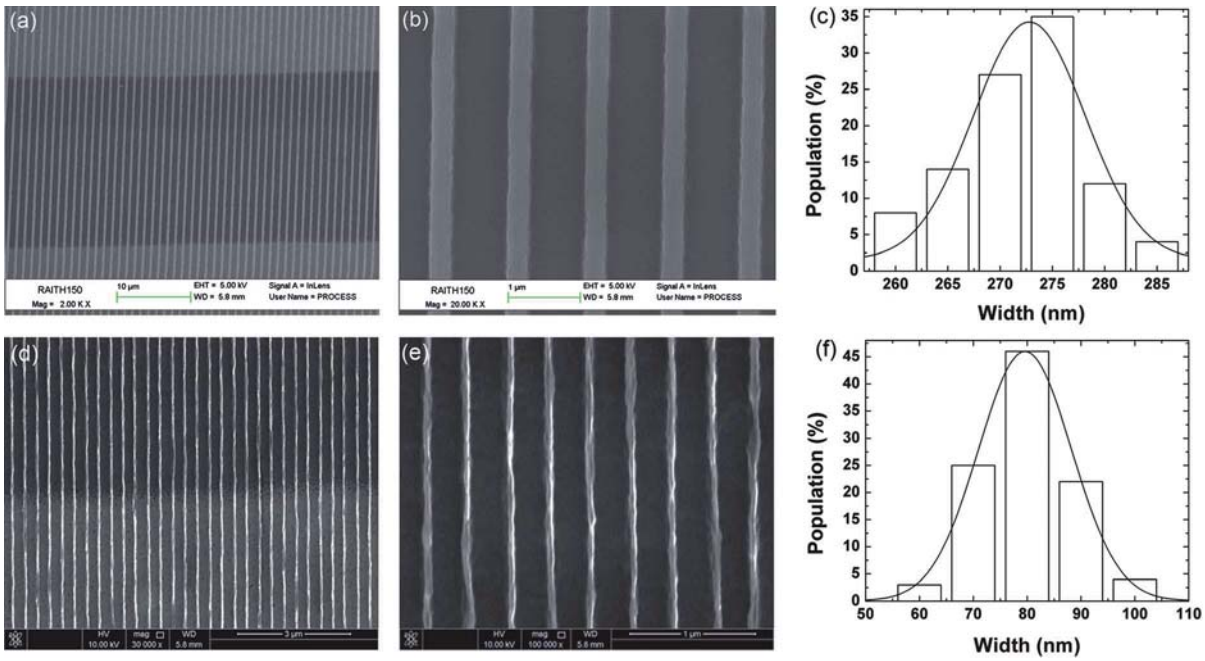


**Fig. 2** Morphological investigation. SEM micrographs of the P3HT 1 μm (a and b) and 330 nm (d and e) periodic patterns on the Au electrodes (light gray region in a and d) and on the $SiO_2$ dielectric (dark gray region). The longitudinal axis of each P3HT feature forms an angle of (87 ± 2)° with the electrodes. (c and f) Width distributions of the features. The superimposed lines are the fits by Gaussian curves.

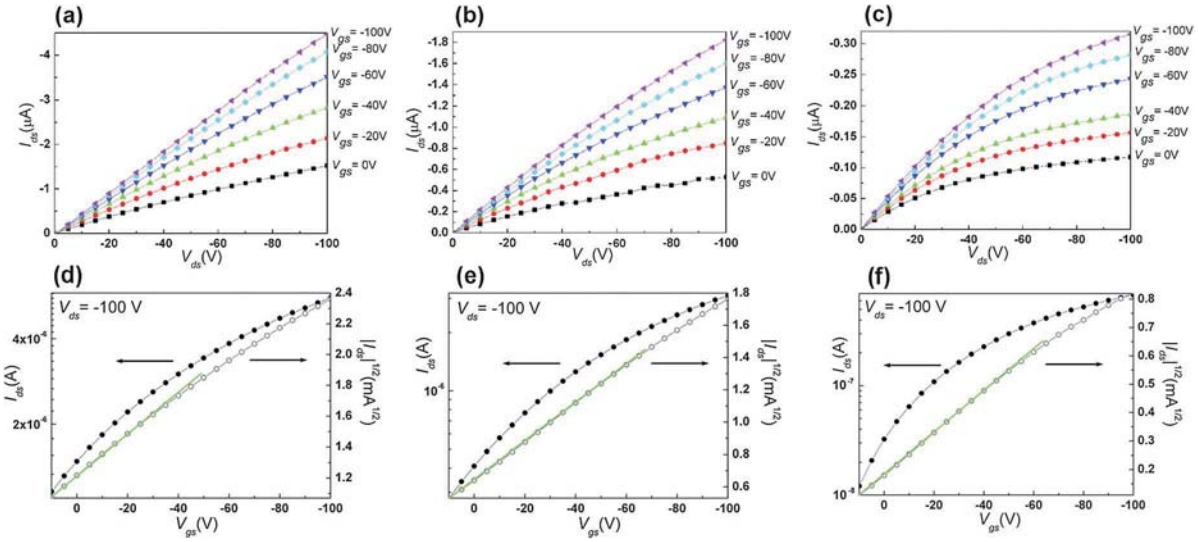


**Fig. 3** Demonstration of OFET with enhanced performance. Output characteristics of OFETs patterned with features of 80 nm (a) and 270 nm (b), and thin-film reference OFETs (c) for various gate bias, $V_{gs} = 0$ V (squares), −20 V (circles), −40 V (upward triangles), −60 V (downward triangles), −80 V (diamonds), and −100 V (leftward triangles). (d–f) Corresponding transfer characteristics $I_{ds}(V_{gs})$ (left vertical scale) and $|I_{ds}|^{1/2}(V_{gs})$ (right vertical scale), for $V_{ds} = -100$ V. Continuous lines: linear fits to data.



than that found for films ($3 \times 10^{-3}$ S m$^{-1}$). An increment of mobility and conductivity with respect to films is also observed for 270 nm structured devices, that exhibit $\mu = 3.5 \times 10^{-2}$ cm$^2$ V$^{-1}$ s$^{-1}$ and $\sigma = 6 \times 10^{-2}$ S m$^{-1}$ (for OFETs patterned by PFPE), or $\mu = 1.1 \times 10^{-2}$ cm$^2$ V$^{-1}$ s$^{-1}$ and $\sigma = 2 \times 10^{-2}$ S m$^{-1}$ (for OFETs patterned by PDMS) replicas. In fact, the relatively lower mobility and conductivity of devices fabricated by using PDMS molds can be related to the presence of the residual layer between the features. Hence, we demonstrate an improvement of the electrical properties of P3HT nanostructured by the soft lithographic approach based on solvent-resistant molds, also in comparison with conventional elastomeric stamps. Furthermore, the field-effect mobility and the conductivity increase upon increasing the pattern resolution, highlighting the effective role played by the employed patterning procedure.

In order to investigate the molecular organization in the nanostructures, we perform grazing-incidence wide-angle X-ray scattering (GIWAXS) measurements. In Fig. 4, GIWAXS two-dimensional (2D) patterns are displayed for 270 nm features obtained by PDMS (Fig. 4a) and by PFPE molds (Fig. 4b), and for 80 nm features obtained by PFPE molds (Fig. 4c). In the 2D patterns, the X-ray scattered intensity is plotted against the scattering vector ($Q$) components, parallel ($Q_r$) and perpendicular ($Q_z$) to the sample surface (strictly speaking the vertical axis represents the total scattering vector, but it has been approximated with its $z$ component due to the small range of scattering angles). For all the analyzed samples, the well-defined (100) series along $Q_z$ indicate that the lamellar stacking direction is preferentially oriented along the surface normal direction, and the presence of the (010) peak along $Q_r$ highlights that the directions of π–π stacking and side chains separation are parallel to the substrate.[17] Hence, P3HT polymer chains preferentially exhibit an edge-on orientation. No significant change in the GIWAXS pattern is observed by changing the in-plane orientation of the features with respect to the incident X-ray beam. Considering the position of the (100) and (010) peaks in the out-of-plane and in-plane profiles (Fig. S3†), we estimate the lattice parameters: $a$ (the distance between the backbones), and $b$ (π-stacking distance) ≅ $c$/2 (separation between the side chains), which are approximately (1.67 ± 0.03) nm and (0.38 ± 0.02) nm, respectively, as typical of P3HT self-assembly.[15] The broad ring around 1.6 Å$^{-1}$ in Fig. 4c can be attributed to the residual presence of randomly oriented P3HT domains, with a possible contribution of the underlying $SiO_2$ substrate on the smaller $Q$ side of the peak.[29] Nonetheless, the P3HT structures at high resolution present a degree of edge-on orientation higher than the 270 nm features. The degree of preferential orientation for the different patterned samples is evaluated by comparing the width of the azimuthal distribution of orientations. The (100) peak intensity is plotted for each GIWAXS map as a function of the azimuthal angle ($\varphi$), defined on the 2D map as the angle between the scattering vector and the horizontal axis. The resulting plots, shown in Fig. 4d, correspond to rocking curves in the ($Q_r$, $Q_z$) plane. We observe that P3HT structures with 270 nm width, obtained by using both PDMS (diamonds) and PFPE molds (circles), are characterized by a comparable degree of orientation with a FWHM of about 25°, whereas for 80 nm P3HT features (triangles) a FWHM of about 15° is measured. This suggests that a more evident edge-on orientation of the P3HT molecules is induced by increasing the pattern resolution, as also demonstrated by the observed increment of the field-effect mobility.

During the soft lithographic procedure, the chains of the regioregular P3HT undergo structural conformational changes mainly due to the fluidic motion, the interaction with the PFPE template, and the concomitant solvent evaporation. In the early stage of printing, the liquid solution is forced to fill the cavities of the non-wetting mold, and such nanofluidic motion causes the initial alignment of the polymeric chains along the flow direction.[26] Upon conformable adhesion of the template to the gate dielectric, the liquid remains highly confined into channels

 

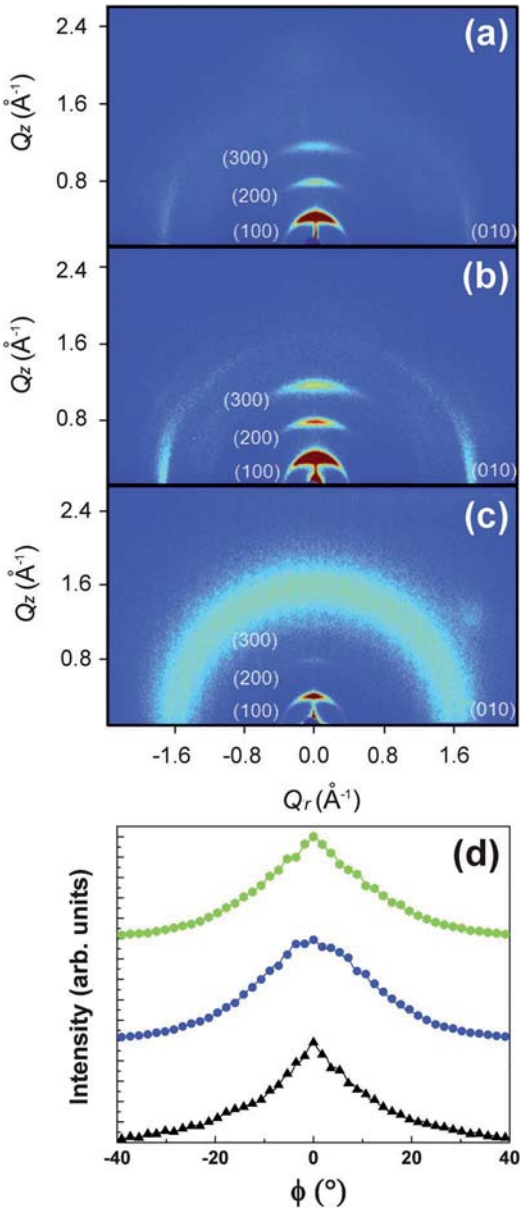


**Fig. 4** GIWAXS analysis of the realized P3HT nanostructures. 2D patterns of 270 nm features obtained by a PDMS mold (a) and a PFPE mold (b), and 80 nm features realized by a PFPE mold (c). (d) Azimuthal profiles of the (100) peak for the different samples: 1 μm periodic pattern produced by PDMS (diamonds) and by PFPE (circles), 330 nm periodic features (triangles).

made of three fluoroelastomer walls and one wall in $SiO_2$. The P3HT molecules rearrange in lamellae having an edge-on orientation, preferentially perpendicular to the channel length, with the π stacking of the conjugated polymer chains along the main axis of the patterned features, that is the direction of the current flow in the device. Moreover, we point out that the use of dichlorobenzene as solvent, due to its high boiling point (180 °C), results in a slow solvent evaporation[30] that facilitates the dynamic molecular self-assembly at the nanoscale before the complete polymer solidification and the mold peeling-off.[19,31]

## Conclusions

In conclusion, the application of these solvent-resistant soft technologies for the processing of conjugated polymers in solution is a promising strategy to realize organic semiconductor devices with highly improved charge transport. We demonstrate isolated features of regioregular P3HT down to below 100 nm, and their application as the active medium in OFETs, obtaining a field-effect mobility 60 times higher with respect to homogeneous films. The high degree of control achieved over the feature dimensions and alignment is of special interest for sensing and optoelectronic devices based on 1D organic nanostructures.

## Acknowledgements

The authors thank Dr F. Di Benedetto and Prof. R. Cingolani for useful discussion, and Dr A. Della Torre for SEM investigation. This work is performed in the framework of the FIRB RBFR08DJZI "Futuro in Ricerca" and partially supported by the SEED project "X-ray synchrotron class rotating anode microsource for the structural micro imaging of nanomaterials and engineered biotissues (XMI-LAB)" – IIT Protocol no. 21537 of 23/12/2009. Mr R. Lassandro is acknowledged for his valuable technical support in the XMI-Lab.

## Notes and references

1 S. Allard, M. Forster, B. Souharce, H. Thiem and H. Scherf, *Angew. Chem., Int. Ed.*, 2008, **47**, 4070–4098.
2 M. Mas-Torrent and C. Rovira, *Chem. Rev.*, 2011, **111**, 4833–4856.
3 G. Derue, D. A. Serban, Ph. Leclère, S. Melinte, P. Damman and R. Lazzaroni, *Org. Electron.*, 2008, **9**, 821–828.
4 D. Tu, S. Pagliara, A. Camposeo, L. Persano, R. Cingolani and D. Pisignano, *Nanoscale*, 2010, **2**, 2217–2222.
5 D. Cui, H. Li, H. Park and X. Cheng, *J. Vac. Sci. Technol., B: Microelectron. Nanometer Struct.–Process., Meas., Phenom.*, 2008, **26**, 2404–2409.
6 Z. Hu, B. Muls, L. Gence, D. A. Serban, J. Hofkens, S. Melinte, B. Nysten, S. Demoustier-Champagne and L. M. Jonas, *Nano Lett.*, 2007, **7**, 3639–3644.
7 D. A. Serban, P. Greco, S. Melinte, A. Vlad, C. A. Dutu, S. Zacchini, M. C. Iapalucci, F. Biscarini and M. Cavallini, *Small*, 2009, **5**, 1117–1122.
8 J. H. Park, S. J. Kang, J. W. Park, B. Lim and D. Y. Kim, *Appl. Phys. Lett.*, 2007, **91**, 222108.
9 Z. Zheng, K. H. Yim, M. S. M. Saifullah, M. E. Welland, R. H. Friend, J. S. Kim and W. T. S. Huck, *Nano Lett.*, 2007, **7**, 987–992.
10 J. N. Lee, C. Park and G. M. Whitesides, *Anal. Chem.*, 2003, **75**, 6544–6554.
11 J. P. Rolland, B. W. Maynor, L. E. Euliss, A. E. Exner, G. M. Denison and J. M. DeSimone, *J. Am. Chem. Soc.*, 2005, **127**, 10096–10100.
12 F. S. Kim, G. Ren and S. A. Jenekhe, *Chem. Mater.*, 2011, **23**, 682–732.
13 S. Pagliara, A. Camposeo, A. Polini, R. Cingolani and D. Pisignano, *Lab Chip*, 2009, **9**, 2851–2856.
14 C. D. Dimitrakopoulos and P. R. L. Malenfant, *Adv. Mater.*, 2002, **14**, 99–117.
15 H. Sirringhaus, P. J. Brown, R. H. Friend, M. M. Nielsen, K. Bechgaard, B. M. W. Langeveld-Voss, A. J. H. Spiering, R. A. J. Janssen, E. W. Meijer, P. Herwig and D. M. De Leeuw, *Nature*, 1999, **401**, 685–688.
16 M. Aryal, K. Trivedi and W. Hu, *ACS Nano*, 2009, **3**, 3085–3090.
17 H. Hlaing, X. Lu, T. Hofmann, K. G. Yager, C. T. Black and B. M. Ocko, *ACS Nano*, 2011, **5**, 7532–7538.
18 G. Wang, J. Swensen, D. Moses and A. J. Heeger, *J. Appl. Phys.*, 2003, **93**, 9208–9211.

19 J. Liu, Y. Sun, X. Gao, R. Xing, L. Zheng, S. Wu, Y. Geng and Y. Han, *Langmuir*, 2011, **27**, 4212–4219.
20 Z. Bao, A. Dodabalapur and A. Lovinger, *Jpn. J. Appl. Phys., Part 2*, 1996, **69**, 4108.
21 D. M. Russell, C. J. Newsome, S. P. Li, T. Kugler, M. Ishida and T. Shimoda, *Appl. Phys. Lett.*, 2005, **87**, 222109.
22 D. D. Schroepfer, P. P. Ruden, Y. Xia, C. D. Frisbie and S. E. Shaheen, *Appl. Phys. Lett.*, 2008, **92**, 013305.
23 M. J. Hampton, S. S. Williams, Z. Zhou, J. Nunes, D. H. Ko, J. L. Templeton, E. T. Samulski and J. M. DeSimone, *Adv. Mater.*, 2008, **20**, 2667–2673.
24 D. Tu, S. Pagliara, A. Camposeo, G. Potente, E. Mele, R. Cingolani and D. Pisignano, *Adv. Funct. Mater.*, 2011, **21**, 1140–1145.
25 E. Mele, A. Camposeo, M. De Giorgi, F. Di Benedetto, C. De Marco, V. Tasco, R. Cingolani and D. Pisignano, *Small*, 2008, **4**, 1894–1899.
26 C. De Marco, E. Mele, A. Camposeo, R. Stabile, R. Cingolani and D. Pisignano, *Adv. Mater.*, 2008, **20**, 4158–4162.
27 S. S. Williams, S. Retterer, R. Lopez, R. Ruiz, E. T. Samulski and J. M. DeSimone, *Nano Lett.*, 2010, **10**, 1421–1428.
28 S. Nagamatsu, W. Takashima and K. Kaneto, *Macromolecules*, 2003, **36**, 5252–5257.
29 S. Joshi, S. Grigorian, U. Pietsch, P. Pingel, A. Zen, D. Neher and U. Scherf, *Macromolecules*, 2008, **41**, 6800–6808.
30 G. Li, Y. Yao, H. Yang, V. Shrotriya, G. Yang and Y. Yang, *Adv. Funct. Mater.*, 2007, **17**, 1636–1644.
31 F. C. Chen, H. C. Tseng and C. J. Ko, *Appl. Phys. Lett.*, 2008, **92**, 103316.



 